*J Mater Sci* (2017) 52:1246–1254

# High formability of glass plus fcc-Al phases in rapidly solidified Al-based multicomponent alloy

F. F. Han[1], A. Inoue[1,2,3,4,*], Y. Han[1], F. L. Kong[2], S. L. Zhu[1], E. Shalaan[3], and F. Al-Marzouki[3]

[1] School of Materials Science and Engineering, Tianjin University, Tianjin, China
[2] International Institute of Green Materials, Josai International University, Togane 283-8555, Japan
[3] Department of Physics, King Abdulaziz University, Jeddah 22254, Saudi Arabia
[4] MISiS, National University of Science and Technology, Moscow, Russia 119049

**Received:** 18 July 2016
**Accepted:** 7 September 2016
**Published online:** 22 November 2016

© Springer Science+Business Media New York 2016

## ABSTRACT

A multicomponent $Al_{84}Y_9Ni_4Co_{1.5}Fe_{0.5}Pd_1$ alloy was found to keep a mixed glassy + Al phases in the relatively large ribbon thickness range up to about 200 μm for the melt-spun ribbon and in the diameter range up to about 1100 μm for the wedge-shaped cone rod prepared by injection copper mold casting. The glassy phase in the Al-based alloy has a unique crystallization process of glass transition, followed by supercooled liquid region, fcc-Al + glass, and then Al + $Al_3Y$ + $Al_9$ $(Co, Fe)_2$ + unknown phase. It is also noticed that the primary precipitation phase from supercooled liquid is composed of an Al phase instead of coexistent Al + compound phases, being different from the crystallization mode from supercooled liquid for ordinary Al-based glassy alloys. In addition, it is noticed that the mixed Al and glassy phases are extended in a wide heating temperature range of 588–703 K, which is favorable for the development of high-strength nanostructure Al-based bulk alloys obtained by warm extrusion of mixed Al + amorphous phases. The Vickers hardness is about 415 for the glassy phase and increases significantly to about 580 for the mixed Al and glassy phases. The knowledge of forming Al + glassy phases with high hardness in the wide solidification and annealing conditions through high stability up to complete crystallization for the multicomponent alloy is promising for future development of a high-strength Al-based bulk alloy.

## Introduction

Nowadays there has been a strong demand of developing a high specific strength and high ductility material consisting mainly of metallic elements which are abundant in Earth's crust. Al-based high-strength alloys are one of the metallic materials which are being developed for many years on the basis of the above-described demand. Although a variety of strengthening mechanisms such as solid solution, grain size refinement, work hardening, precipitation hardening, and dispersion strengthening are well

Address correspondence to E-mail: inoue@jiu.ac.jp



DOI 10.1007/s10853-016-0394-6

known for conventional Al-based alloys [1, 2], some new types of strengthening mechanisms as exemplified for fine quasicrystal dispersion [3, 4], nanocrystalline composite [5], primary precipitation compound dispersion [6], and amorphization [7–10] have also been reported for the last two decades. As a result, the nanocrystalline composite and the primary precipitation compound alloys have gained wide applications such as structural, machinery, mold, and sports goods materials [9, 11, 12]. When we focus on high strength of Al-based alloys [13, 14], the highest strength has been obtained for two kinds of phases, namely, glassy phase and nanoscale Al + glass phases. Their highest tensile strength value at room temperature reaches 1505 MPa for $(Al_{0.84}Y_{0.09}Ni_{0.05}Co_{0.02})_{95}Sc_5$ glassy alloy [15] and 1550 MPa for $Al_{88}Fe_1Ce_2Ni_9$ alloy consisting of Al + glassy phases [16].

In addition, the highest glass-forming ability has been reported for Al–Y–Ni–Co base alloy systems containing additional special elements such as Sc [17] and La [18]. Thus, it is notable that the base alloy system to achieve the highest glass-forming ability is Al–Y–Ni–Co quaternary alloy for both the cases, though their data were obtained in different research groups. It is therefore important to develop a new Al-based glassy alloy with high strength and high glass-forming ability or high forming ability of Al + glassy phases on the basis of the Al–Y–Ni–Co alloy system. When we look at the crystallization behavior of Al–Y–Ni–Co glassy alloy, the alloy is subjected to continuous heating crystallization through the transition process of glass transition, supercooled liquid, and then co-precipitation of Al + $Al_3Y$ + $Al_3TM$ (TM = Ni and Co) [19–23]. Thus, Al-based glassy alloys with glass transition and supercooled liquid region ordinarily crystallizes through the simultaneous precipitation of Al and compounds from supercooled liquid. There have been few literatures about the formation and crystallization behavior of Al-based glassy alloys with glass transition, followed by supercooled liquid and then primary Al-phase precipitation, though active and extensive studies on Al-based amorphous and glassy alloys have been carried out [9] since the first synthesis of high-strength Al-based glassy alloy in 1988 [7–9, 24]. Besides, there are some papers on the influence of minor addition of Pd [25] or Fe [26] on the stability of supercooled liquid region and crystallization behavior of Al–Y–Ni–Co base glassy alloys. The addition of each element reduces the supercooled liquid region but does not have any useful effect for the increase in glass-forming ability.

Very recently, we have found that the coexistent Al + glassy phases can be formed in wide rapid solidification conditions and are also maintained in a wide heating temperature range from 588 to 703 K during crystallization from supercooled liquid for Al–Y–Ni–Co–Fe–Pd multicomponent glassy alloys. This paper aims to present the formation and crystallization behavior of $Al_{84}Y_9Ni_4Co_{1.5}Fe_{0.5}Pd_1$ glassy alloy and the feature of coexistent Al + glassy phases, and to investigate the reason why the Al-based glassy alloy has a rather high glass-forming ability with thicknesses above 200 μm in the melt spinning process as well as the primary Al precipitation mode from supercooled liquid instead of the co-precipitation crystallization mode.

## Experimental procedure

An Al-based alloy with nominal atomic composition of $Al_{84}Y_9Ni_4Co_{1.5}Fe_{0.5}Pd_1$ was chosen because the highest glass-forming ability in Al-based quaternary alloys was obtained for $Al_{84}Y_9Ni_5Co_2$ alloy [19] and the additional Y–Pd and Y–Fe atomic pairs have very large negative heats of mixing [20]. The mother alloy was prepared by arc melting the mixture consisting of pure metals with high purities above 99.9 mass% in an argon atmosphere. Ribbon samples with different thicknesses and a width of about 1.5 mm were prepared by melt spinning with a copper wheel of 250 mm in diameter in an argon atmosphere. The circumferential velocity of the wheel was changed in the range of 3.9–44 m/s and the thickness of the resulting ribbons was 200–20 μm, respectively. In addition, a wedge-shaped cone rod with an angle of 5° at the top edge and a length of 40 mm was prepared by the injection copper mold casting method in an argon atmosphere. The structures of as-spun ribbons and cast alloy rods were examined by X-ray diffraction with Cu $K_\alpha$ radiation and transmission electron microscopy (TEM). Thermal stability associated with glass transition ($T_g$), crystallization temperature ($T_x$), melting temperature ($T_m$), and liquid temperature ($T_l$) was evaluated by differential scanning calorimetry (DSC) at a heating rate of 0.67 K/s. The structure after annealing was examined by X-ray diffraction, optical microscopy (OM), scanning electron microscopy (SEM), and high-resolution TEM

equipped with a nanobeam EDX analyzer. Hardness was measured by a Vickers hardness tester with a load of 0.245 N. Ductility was evaluated by a simple bending test. The deformation structure was examined by OM and SEM.

## Results

Figure 1 (a) shows X-ray diffraction patterns of melt-spun $Al_{84}Y_9Ni_4Co_{1.5}Fe_{0.5}Pd_1$ alloy ribbons prepared at different wheel speeds of 3.9–44 m/s. All the samples show only broad X-ray diffraction peaks without obvious diffraction peaks due to crystalline phase. However, when we pay attention to the peak position of the main broad peak, the summit position appears to shift slightly to a higher diffraction angle side with increasing the ribbon thickness to 185 μm and significantly for the thick ribbon of 200 μm in thickness and approaches 38.47 degrees for crystalline Al as shown in Fig. 1b, suggesting that the thicker ribbon samples of 185 and 200 μm thickness include small amounts of fine fcc-Al phase. Figure 2a shows DSC curves of the melt-spun Al-based alloy ribbons prepared at different circumferential velocities of 3.9–44 m/s. All the samples show two exothermic peaks. Especially, the ribbon prepared at 44 m/s shows a distinct endothermic reaction due to glass transition, followed by a small supercooled liquid region, sharp high-intensity exothermic peak due to the precipitation of crystalline phase at an onset temperature of 578 K and a peak temperature of 588 K, and then a rather broad exothermic peak with a peak temperature of 703 K. However, as summarized in Fig. 2c, the glass transition temperature ($T_g$) increases gradually in conjunction with the decrease in endothermic reaction and the heat of the first exothermic peak decreases clearly with increasing ribbon thickness, though there is no obvious change in the second exothermic peak with ribbon thickness. The continuous rise of $T_g$ reflects the progress of structural relaxation in the amorphous phase, while the decrease in the heat of the first exothermic peak indicates that the as-spun ribbon includes the precipitation phase (fcc-Al phase as described later) corresponding to the first exothermic peak, being consistent with the X-ray diffraction data shown in Fig. 1. In addition, as shown in Fig. 2b, the absence of the endothermic reaction due to glass transition for the thick ribbon sample of 200 μm in thickness is presumably because the reaction is too small to detect by the ordinary DSC measurement owing to the increase in the volume fraction of fcc-Al precipitates.

With the aim of clarifying the precipitates caused by the first and the second exothermic reactions, Fig. 3 shows X-ray diffraction patterns of the amorphous ribbons annealed for 900 s at 650 and 750 K, which correspond to the temperature between the

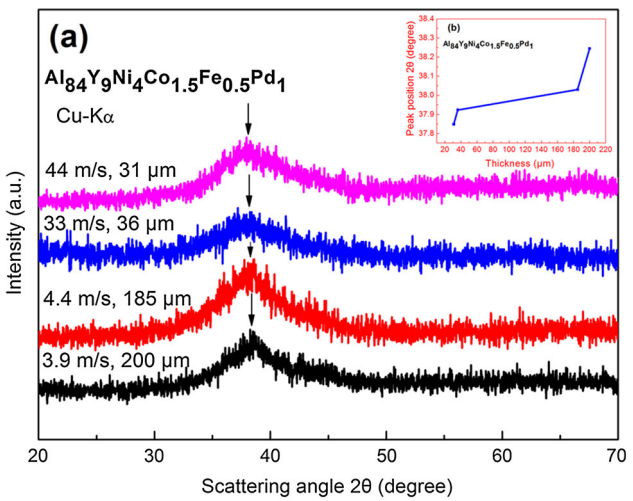


**Figure 1** **a** X-ray diffraction patterns of melt-spun $Al_{84}Y_9Ni_4Co_{1.5}Fe_{0.5}Pd_1$ alloy ribbons with thicknesses of 31–200 μm prepared at different wheel speeds, and (*b*) the change in the peak position of the diffraction patterns with ribbon thickness.

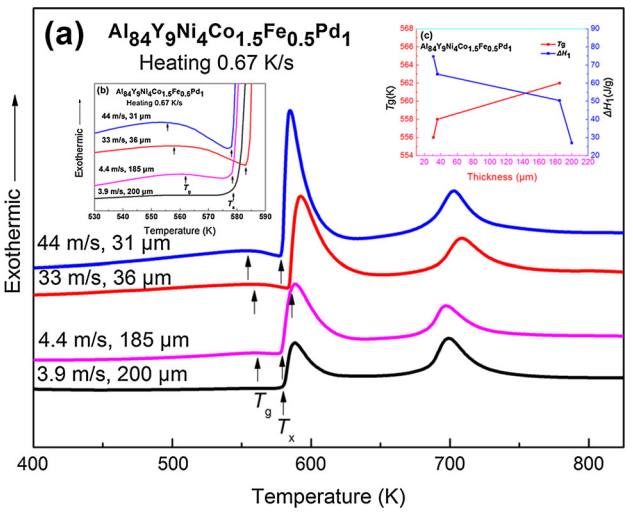


**Figure 2** **a** DSC traces of melt-spun $Al_{84}Y_9Ni_4Co_{1.5}Fe_{0.5}Pd_1$ alloy ribbons with different thicknesses, (*b*) the enlarging image of $T_g$ temperature region, and (*c*) the changes in glass transition temperature ($T_g$) and the heat of the first exothermic peak ($\Delta H_1$) with ribbon thickness.

first exothermic peak and the second one and to the temperature well above the second exothermic peak, respectively. The diffraction peaks of the former annealed alloy can be identified as a mostly single fcc-Al phase with a lattice parameter of 0.406 nm, indicating that the first sharp exothermic peak is due to the precipitation of Al phase. On the other hand, the diffraction pattern of the latter annealed sample consists of Al, $Al_3Y$, $Al_9$ (Co, Fe)$_2$, and unknown phases. Based on these data on DSC and X-ray diffraction patterns, it is concluded that (1) the crystallization of the $Al_{84}Y_9Ni_4Co_{1.5}Fe_{0.5}Pd_1$ glassy alloy occurs through two stages of glass → supercooled liquid → Al + glass → Al + compounds for the ribbon sample with a thickness of 31 μm, (2) with further increase of the ribbon thickness, the as-spun ribbons have a mixed structure consisting of amorphous + Al phases, (3) the precipitation amount of Al phase increases with increasing ribbon thickness, and (4) the amorphous phase can remain even for the thick ribbon with a thickness of about 200 μm.

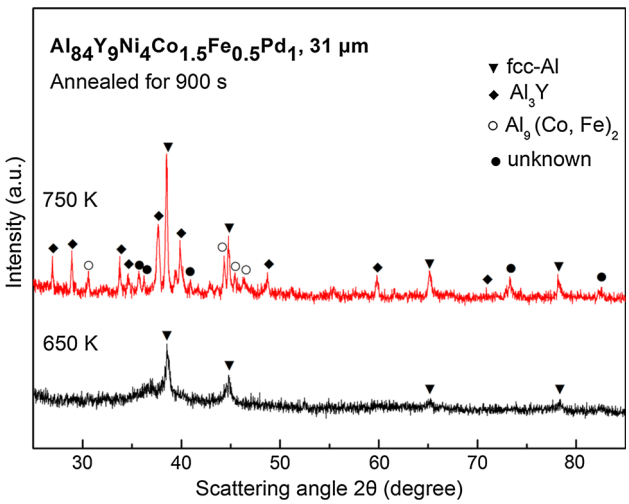


**Figure 3** X-ray diffraction patterns of $Al_{84}Y_9Ni_4Co_{1.5}Fe_{0.5}Pd_1$ glassy alloy ribbons annealed for 900 s at 650 and 750 K and their identification results.

In order to confirm the precipitation of Al phase and to clarify the size and morphology of the Al-phase precipitates, TEM bright-field image, selected-area electron diffraction pattern, and HRTEM image of the Al–Y–Ni–Co–Fe–Pd alloy annealed for 900 s at 650 K are shown in Fig. 4. The diffraction pattern (Fig. 4b) consists mainly of Al diffraction rings and broad halo rings, indicating that the annealed sample is composed of Al and the remaining amorphous phase. As shown in the bright-field images of Fig. 4a, the precipitates of Al phase have a fine size of about 10–20 nm and their morphology appears to be of pseudo-dendritic shape, in contrast to the spherical morphology for Al phase which precipitates from amorphous phase without glass transition [27]. Consequently, the appearance of the very fine pseudo-dendritic Al phase can be regarded as the feature of the precipitation mode from supercooled liquid. It is also noticed that the precipitates of Al phase keep very fine size of 10–20 nm even from the supercooled liquid state where the atomic rearrangement on a long scale can occur. The size is comparable to that of the precipitates from amorphous solid which appear in much lower temperature side [28]. Such a significant suppression effect of grain growth for the Al precipitates from the supercooled liquid seems to be due to the special change for the supercooled liquid, namely, to the difficulty of long-range rearrangement of the multicomponent which is one of the features for multicomponent

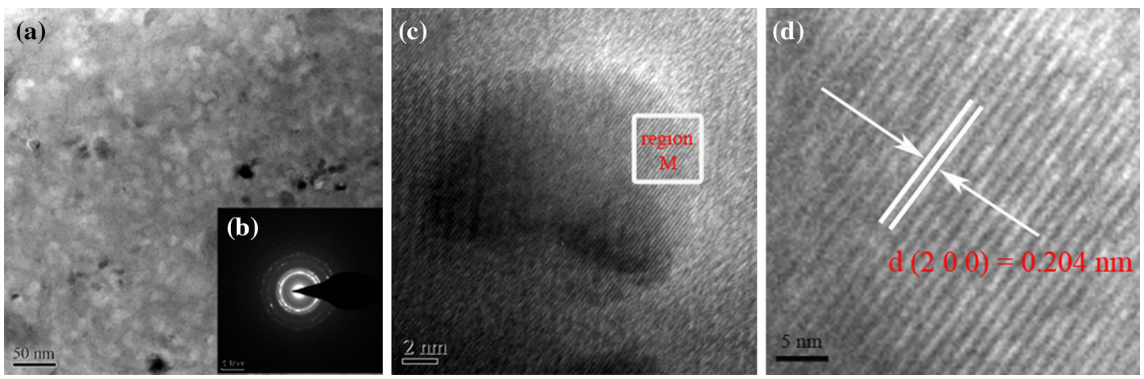


**Figure 4** **a** Bright-field TEM image, **b** selected-area electron diffraction pattern, **c** highly magnified bright-field image, and **d** enlarged image of the region marked with *region M* in **c** for $Al_{84}Y_9Ni_4Co_{1.5}Fe_{0.5}Pd_1$ glassy alloy ribbon annealed for 900 s at 650 K.

glassy alloys [29]. In addition, the lattice parameter of Al phase measured from the reflection rings of Al shown in Fig. 4b and the fringe contrast corresponding to $(002)_{Al}$ shown in Fig. 4d is evaluated to be 0.408 nm. Although the lattice parameter does not agree perfectly with the value (0.406 nm) of Al obtained from the X-ray diffraction pattern shown in Fig. 3, one can notice that the actually measured lattice parameters of Al are slightly larger than that (0.405 nm) [30] of pure Al, indicating that the Al phase precipitated from supercooled liquid dissolves certain amounts of solute elements. Considering that only Y element has larger atomic size than Al [31], the expansion of the lattice parameter is thought to reflect the dissolution of Y element.

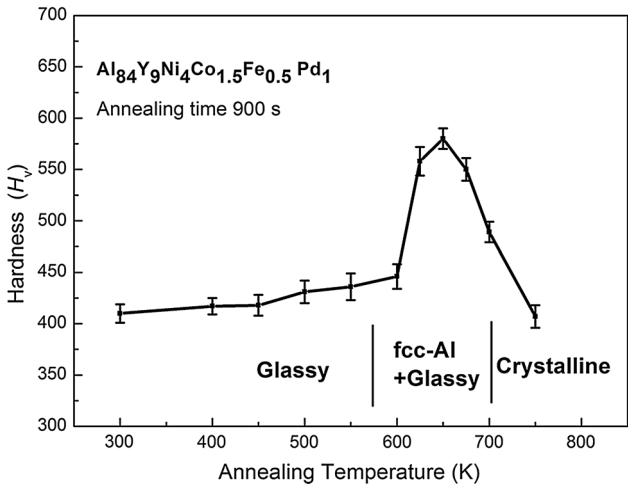


**Figure 5** Changes in Vickers hardness and structure with annealing temperature for $Al_{84}Y_9Ni_4Co_{1.5}Fe_{0.5}Pd_1$ alloy ribbon with a thickness of 31 μm.

Figure 5 shows the change in Vickers hardness with annealing temperature for the Al-based glassy alloy ribbon of about 31 μm in thickness. The hardness is about 415 in the glassy state, increases significantly to 580 in the mixed Al + glassy state, and then decreases to 400 in the fully crystallized state. It is notable that extremely high hardness values exceeding 550 are obtained for the coexistent structure of Al + glassy phases. In addition, even in the high hardness state, one can see some slip markings in the region around the Vickers hardness indenter trace shown in Fig. 6, indicating that the high hardness alloy still keeps appreciable deformability.

As shown in Figs. 1 and 2, the amorphous phase in the melt-spun $Al_{84}Y_9Ni_4Co_{1.5}Fe_{0.5}Pd_1$ alloy ribbon is formed over the whole thickness range up to about 200 μm which is the maximum thickness prepared in the present melt spinning method. This result indicates that the Al-based alloy has a top class of high glass-forming ability among a number of Al-based alloys reported to date [17, 18, 32–34]. This is because no glassy single-phase alloy rod exceeding 1.5 mm in diameter is formed even at present and the data on amorphous + Al-mixed phases are also limited in Al–Y–Ni–Co–Si–Sc alloy rod of about 1 mm in diameter prepared by injection copper mold casting [17].

Considering the previously reported data [27, 32–35], it is important to examine the maximum diameter for the formation of a glassy phase in the alloy rod with the new alloy composition prepared by the same injection casting. Figure 7 shows outer shape, surface morphology, and cross-sectional structure at the depth of 34 mm (at the diameter of

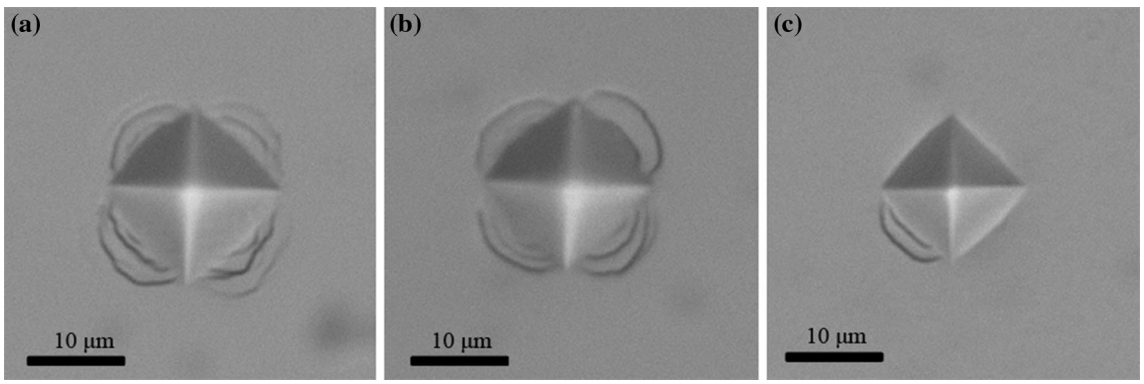


**Figure 6** Optical micrographs revealing the slip deformation marking around the Vickers hardness indentation trace of $Al_{84}Y_9Ni_4Co_{1.5}Fe_{0.5}Pd_1$ glassy alloy ribbon with a thickness of 31 μm. **a** as-spun glassy state, **b** glassy state annealed for 900 s at 550 K and **c** Al + glassy state annealed for 900 s at 650 K.

1.14 mm) for the cast alloy rod with a wedge-type cone shape where the edge angle is 5 degrees and the depth is 40 mm. The distinct contrast typical for the crystalline phase is hardly seen in the optical micrograph shown in Fig. 7b, indicating the formation of a mostly single amorphous phase. It is thus concluded that the maximum diameter for the formation of a mostly single amorphous phase without obvious contrast due to crystalline phase by optical microscopy lies in the vicinity of 1100 μm. Judging from some previous data that the maximum diameter for the formation of amorphous phase is about 720 μm for $Al_{85}Ni_5Y_8Co_2$ [19] and 1500 μm for $Al_{86}Ni_{6.75}Co_{2.25}Y_{3.25}La_{1.75}$ [18], while the maximum one for the formation of amorphous + Al phases is about 1 mm for $Al_{86}Si_{0.5}Ni_{4.06}Co_{2.94}Y_6Sc_{0.5}$ alloy [17], the glass-forming ability of the present alloy is comparable to those for the previously reported Al-based alloys which are known to have the highest glass-forming ability among Al-based glassy alloys.

Figure 8 shows the changes in Vickers hardness and as-cast structure with the distance from the bottom edge for the cast $Al_{84}Y_9Ni_4Co_{1.5}Fe_{0.5}Pd_1$ alloy rod. The hardness value is about 300 in the crystalline state, increases significantly in the coexistence of amorphous + crystalline phases and reaches a maximum of about 450 in the mostly single amorphous phase. The hardness values of the glassy phase are also comparable to those for Al–Y–Ni–Co–Sc glassy alloy ribbons with high tensile strength above

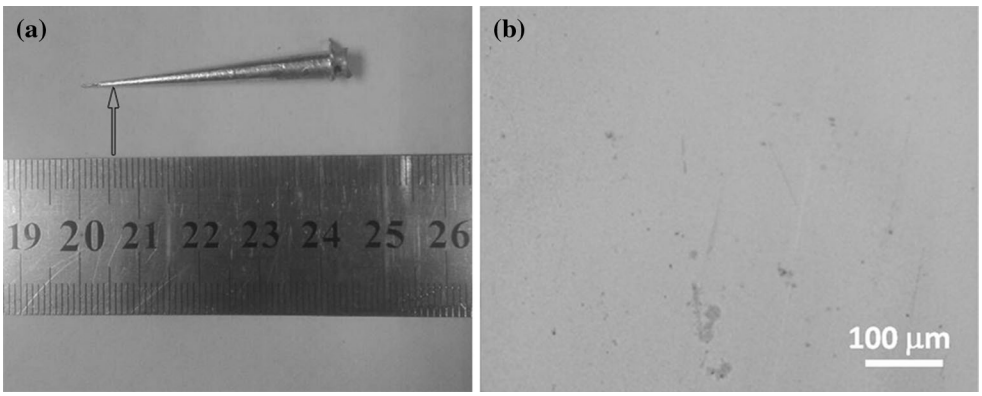


**Figure 7** **a** Outer surface appearance of cast $Al_{84}Y_9Ni_4Co_{1.5}Fe_{0.5}Pd_1$ alloy rod in a wedge shape with edge angle of 5° and the length of 40 mm prepared by injection casting and the *arrow* indicates the site where the cross section was observed, and **b** optical micrographs revealing the cross-sectional structure at the length of 34 mm (at the diameter of 1.135 mm) for the cast edge-shaped alloy rod.

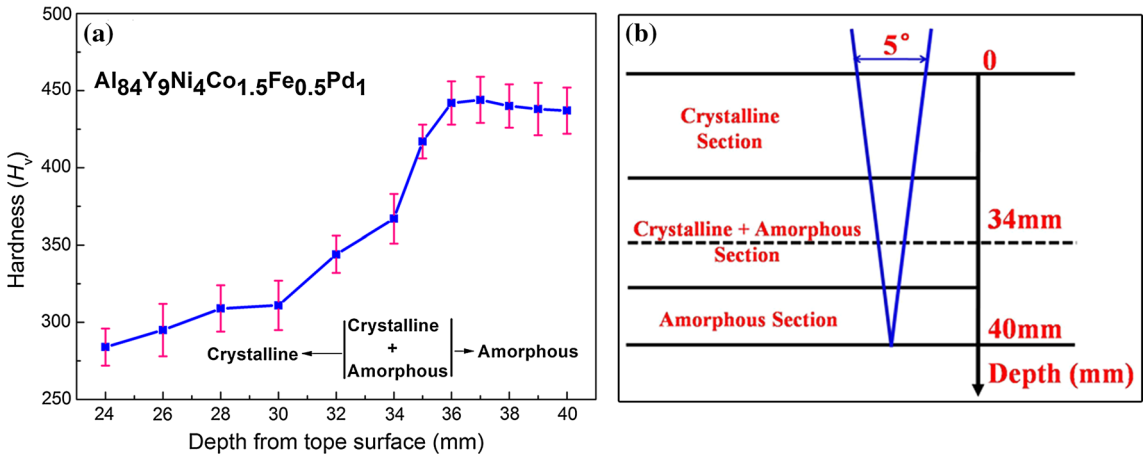


**Figure 8** **a** Changes in Vickers hardness and structure with the distance from the bottom edge for the cast wedge-shaped $Al_{84}Y_9Ni_4Co_{1.5}Fe_{0.5}Pd_1$ alloy rod, and **b** the relation between the as-cast structure and the wedge-shaped cone rod prepared by injection copper mold casting.

1500 MPa [15]. As seen in Figs. 5 and 8, the hardness value of the as-cast amorphous phase is higher by about 10 % than that for the as-spun amorphous phase. The difference is consistent with the general tendency that the higher hardness value is obtained for the thicker sample with more relaxed disordered structure [36].

## Discussion

As shown in Figs. 2 and 3, the present Al-based alloy crystallizes through the sequent change in the glass transition, followed by the supercooled liquid region, sharp crystallization peak due to the precipitation of Al, and then the co-precipitation of Al + $Al_3Y$ + $Al_9(Co, Fe)_2$ + unknown phase from Al + amorphous phases. It is further confirmed by DTA analyses that the melting of the Al-based alloy occurred through a mostly single stage, indicating that the alloy composition is located near the eutectic point. To date, a large number of glassy alloys with glass transition and supercooled liquid region before crystallization have been reported in almost all transition metal base systems [29]. Besides, the primary precipitation phase from supercooled liquid for the glassy-type alloys consists of mixed phases of base metal and compounds or very complex compound-type phases such as icosahedral, big cubic $\chi$, and complex cubic $M_{23}B_6$ [35, 37, 38], and no base metal crystalline phase such as fcc, bcc, and hcp phases has been reported as the primary precipitation phase from supercooled liquid region where the long-range atomic rearrangement occurs easily, though such base metal crystalline phases can precipitate rather easily from the amorphous-type phase without glass transition and supercooled liquid region before crystallization. The present new observation result also indicates that the supercooled liquid has extremely high resistance to the precipitation of Al-based compound phases. The precipitation mode of Al phase from supercooled liquid is also different from the ordinary precipitation mode of Al, as is evident from a number of previous data that the primary exothermic peak due to the precipitation of base metal phase has a relatively broad shape with long tail which corresponds to the easy nucleation and slow grain growth [39].

In comparison with the above-described previous general information of crystallization for glassy alloys [39], it is concluded that the present Al-based glassy alloy has an extremely abnormal decomposition behavior of glassy and/or supercooled liquid phases. In addition, the remaining glassy phase can maintain in the high temperature range up to about 703 K. Thus, the glassy phase in the present Al-based alloy also has very high thermal stability to the completion of crystallization. Although the definite reason for such an abnormal crystallization behavior is unknown in the limited study, the following two reasons may be considered; (1) the coexistence of Y and Pd elements, and (2) the effect of multicomponent. Among the atomic pairs in the Al–Y–Ni–Co–Fe–Pd glassy alloy, the negative heat of mixing is −46 kJ/mol for Al–Pd pair and −84 kJ/mol for Y–Pd pair which are much larger than those for all other atomic pairs [20]. The largest negative heat of mixing for Y–Pd atomic pair indicates the possibility that the preferential atomic bonding of Y–Pd causes the generation of Al-rich atomic pairs through the apparent reduction of solute content which enables the primary precipitation of Al phase. In addition, the multicomponent composition including Pd with larger negative heats of mixing as well as Y with much larger atomic size can suppress the long-range rearrangements of their constituent elements, resulting in the appearance of $T_g$ and the high stability of Al + glass-mixed phases. It is thus presumed that the unique multicomponent including Pd and Y with extremely large negative heats of mixing and large atomic size mismatches causes the present abnormally stable mixed structure consisting of glassy + Al phases. The further researches along the present interpretation are expected to enable the development of a new Al-based glassy alloy with much stable glassy + Al-mixed phases. It is finally important to point out that the development of Al-based glassy alloy with $T_g$ and highly stable Al + glass phases is very valuable for the formation of nanoscale-mixed structures such as Al + amorphous and Al + nanoscale compound in a bulk form using warm extrusion or hot pressing treatments in the Al + amorphous-mixed state, as is evidenced from the result that the bulk Al-based alloys consisting of Al + nanoscale compounds ($Al_3Ni$ + $Al_3(Ce, Zr)$) in Al–Ni–Ce–Zr system had been used as commercial high-strength materials in the wide fields of structural, sporting goods, tool, mold, machining, robotic, bicycle, and wheelchair parts [9, 40].

## Summary

The multicomponent effect of alloy component on the thermal stability and crystallization process was examined for typical glass-type Al–Y–Ni–Co-based alloy. It was found that the multicomponent Al–Y–Ni–Co–Fe–Pd glassy alloy containing elements with large negative heats of mixing and significant atomic size mismatches can have the mixed structure of glassy + Al phases in the thickness range up to about 200 μm for melt spinning and in the diameter range below about 1100 μm for injection casting to copper mold. The single glassy alloy ribbons below 31 μm in thickness exhibit the glass transition and supercooled liquid region, and then crystallize through the process of Al + glass → Al + $Al_3Y$ + $Al_9(Co, Fe)_2$ + unknown phase. The coexistent Al + glass phase region is also extended in a wide heating temperature range of 588–703 K. The precipitation of only Al phase from the supercooled liquid is different from the previous crystallization mode of simultaneous precipitations of more than two phases including compounds which have been generally recognized for glass-type alloys. The formation of coexistent Al + glassy phases in wide as-spun and as-cast precipitation conditions as well as in the wide temperature interval of about 115 K in the heating-induced crystallization process is useful for basic knowledge to develop a high-strength Al-based bulk alloy with nanocrystalline structure.

## Acknowledgments

The present research is supported by Recruitment Program of Global Experts "1000 Talents Plan" of China (WQ20121200052), JSPS KAKENHI Grant Number 26630299 in Japan, Deanship of Scientific Research (DSR), King Abdulaziz University, Jeddah, Saudi Arabia (1-1-1435/HiCi), and the Ministry of Education and Science of the Russian Federation in the framework of the Program aimed to increase the competitiveness of the National University of Science and Technology "MISiS" (No.K1-2015-026).

## Compliance with ethical standards

**Conflict of interest** The authors declare no conflict of interest.

## References

[1] Davis JR (1993) Aluminum and aluminum alloys, ASM international

[2] Malek P, Janecek M, Smola B, Bartuska P, Plestil J (2000) Structure and properties of rapidly solidified Al–Zr–Ti alloys. J Mater Sci 35:2625–2633

[3] Inoue A, Kimura H (2000) High-strength aluminum alloys containing nanoquasicrystalline particles. Mat Sci Eng 286:1–10

[4] Zhu M, Yang GC, YaoLJ Cheng SL, Zhou YH (2010) Microstructure and mechanical properties of Al-base composites by addition of Al–Ni–Co decagonal quasicrystalline particles through a mechanical stirring route. J Mater Sci 45:3727–3734

[5] Taketani K, Uoya A, Ohtera K, Uehara T, Higashi K, Inoue A (1994) Readily superplastic forging at high strain rates in an aluminium-based alloy produced from nanocrystalline powders. J Mater Sci 29:6513–6517

[6] Tokuoka T, Kaji T, Nishioka T, Ikegaya A (2006) Development of high-strength, heat-resistant aluminum alloy made by powder forging process. SEI Technical Review 61:70–76

[7] Inoue A, Yamamoto M, Kimura HM, Masumoto T (1987) Ductile aluminium-base amorphous alloys with two separate phases. J Mater Sci Lett 6:194–196

[8] He Y, Poon SJ, Shiflet GJ (1988) Synthesis and properties of metallic glasses that contain aluminum. Science 241:1640–1642

[9] Inoue A (1998) Amorphous, nanoquasicrystalline and nanocrystalline alloys in Al-based systems. Prog Mater Sci 43:365–520

[10] Scudino S, Surreddi KB, Sager S, Sakaliyskaet M, Kim JS, Loser W, Eckert J (2008) Production and mechanical properties of metallic glass-reinforced Al-based metal matrix composites. J Mater Sci 43:4518–4526

[11] Nieh TG, Wadsworth J (1991) High-strain-rate superplasticity in aluminum matrix composites. Mat Sci Eng 147:129–142

[12] Inoue A, Kimura H, Amiya K (2002) Developments of aluminum- and magnesium-based nanophase high-strength alloys by use of melt quenching-induced metastable phase. Mater Trans 43:2006–2016

[13] Gordillo MA, Cernatescu I, Aindow TT, Watson TJ, Aindow M (2014) Phase stability in a powder-processed Al–Mn–Ce alloy. J Mater Sci 49:3742–3754

[14] Calin M, Grahl H, Adam M, Eckert J, Schultzl L (2004) Synthesis and thermal stability of ball-milled and melt-quenched amorphous and nanostructured Al–Ni–Nd–Co alloys. J Mater Sci 39:5295–5298

[15] Inoue A, Sobu S, Louzguine DV, Kimura H, Sasamori K (2004) Ultrahigh strength Al-based amorphous alloys containing Sc. J Mater Res 19:1539–1543

[16] Inoue A, Horio Y, Kim Y, Masumoto T (1992) Elevated-temperature strength of an $Al_{88}Ni_9Ce_2Fe_1$ amorphous alloy containing nanoscale fcc-Al particles. Mater Trans, JIM 33:669–674

[17] Zhuo L, Pang S, Wang H, Zhang T (2009) Ductile bulk aluminum-based alloy with good glass-forming ability and high strength. Chin Phys Lett 26:066402

[18] Wu NC, Zuo L, Wang JQ, Ma E (2016) Designing aluminum-rich bulk metallic glasses via electronic-structure-guided microalloying. Acta Mater 108:143–151

[19] Inoue A, Matsumoto N, Masumoto T (1990) Al–Ni–Y–Co amorphous alloys with high mechanical strengths, wide supercooled liquid region and large glass-forming capacity. Mater Trans, JIM 31:493–500

[20] Takeuchi A, Inoue A (2005) Classification of bulk metallic glasses by atomic size difference, heat of mixing and period of constituent elements and its application to characterization of the main alloying element. Mater Trans 46:2817–2829

[21] Louzguine DV, Inoue A (2002) Influence of a supercooled liquid on crystallization behaviour of Al–Y–Ni–Co metallic glass. Mater Lett 54:75–80

[22] Bassim N, Kiminami CS, Kaufman MJ, Oliveira MF, Perdigao MNRV, Botta Filho WJ (2001) Crystallization behavior of amorphous $Al_{84}Y_9Ni_5Co_2$ alloy. Mater Sci Eng 304:332–337

[23] Nitsche H, Sommer F, Mittemeijer EJ (2005) The Al nanocrystallization process in amorphous $Al_{85}Y_8Ni_5Co_2$. J Non-Cryst Solids 351:3760–3771

[24] Louzguine D, Inoue A (2002) Crystallization behaviour of Al-based metallic glasses below and above the glass-transition temperature. J Non-Cryst Solids 311:281–293

[25] Inoue A, Ohtera K, Tsai A-P, Masumoto T (1988) Aluminum-based amorphous alloys with tensile strength above 980 MPa (100 kg/mm$^2$). Jpn J Appl Phys 27:L479

[26] Louzguine DV, Inoue A (2001) Full or particle replacement of Y by rare-earth and some other elements in the $Al_{85}Y_8Ni_5Co_2$ alloy. J Light Met 1:105–109

[27] Kim HY, Inoue A, Masumoto T (1991) Ultrahigh mechanical strengths of $Al_{88}Y_2Ni_{10-x}M_x$ (M = Mn, Fe or Co) amorphous alloys containing nanoscale fcc-Al particles. Mater Trans, JIM 32:599–608

[28] Inoue A, Nakazato K, Kawamura Y, Tsai A, Masumoto T (1994) Effect of Cu or Ag on the formation of coexistent nanoscale Al particles in Al–Ni–M–Ce (M = Cu or Ag) amorphous alloys. Mater Trans, JIM 35:95–102

[29] Inoue A (2000) Stabilization of metallic supercooled liquid and bulk amorphous alloys. Acta Mater 48:279–306

[30] Xie YQ, Peng K, Liu XB (2004) Influences of xTi/xAl on atomic states, lattice constants and potential-energy planes of ordered FCC TiAl-type alloys. Phys B 344:5–20

[31] Inoue A, Ohtera K, Masumoto T (1988) New amorphous Al–Y, Al–La and Al–Ce alloys prepared by melt spinning. Jpn J Appl Phys 27:736–739

[32] Louzguine DV, Inoue A (2002) Investigation of structure and properties of the Al–Y–Ni–Co–Cu metallic glasses. J Mater Res 17:1014–1018

[33] Yang H, Dong P, Wang J, Li Y (2007) Glass formability and structural stability of Al-based alloy systems. Mat Sci Eng A-Struct 449:273–276

[34] Wang JQ, Liu YH, Imhoff S, Chen N, Louzguine-Luzgin DV, Takeuchi A, Chen MW, Kato H, Perepezko JH, Inoue A (2012) Enhance the thermal stability and glass forming ability of Al-based metallic glass by Ca minor-alloying. Intermetallics 29:35–40

[35] Hirata A, Hirotsu Y, Amiya K, Nishiyama N, Inoue A (2009) $Fe_{23}B_6$-type quasicrystal-like structures without icosahedral atomic arrangement in an Fe-based metallic glass. Phys Rev B 80:140201

[36] Saida J, Yamada R, Wakeda M (2013) Recovery of less relaxed state in Zr–Al–Ni–Cu bulk metallic glass annealed above glass transition temperature. Appl Phys Lett 103:221910

[37] Hirata A, Hirotsu Y, Amiya K, Inoue A (2010) Quasicrystal-like structure and its crystalline approximant in an $Fe_{48}Cr_{15}Mo_{14}C_{15}B_6Tm_2$ bulk metallic glass. J Alloy Compd 504:186–189

[38] Louzguine DV, Bazlov AI, Ketov SV, Greer AL, Inoue A (2015) Crystal growth limitation as a critical factor for formation of Fe-based metallic glasses. Acta Mater 82:396–402

[39] Bassim N, Kiminami CS, Kaufman MJ (2000) Phases formed during crystallization of amorphous $Al_{84}Y_9Ni_5Co_2$ alloy. J Non-Cryst Solids 273:271–276

[40] Inoue A, Kong FL, Zhu SL, Liu CT (2015) Development and applications of highly functional Al-based materials by use of metastable phases. Mater Res 18:1414–1425